Journal of the European Optical Society - Rapid Publications 5, 10021 (2010) www.jeos.org

Application of the method of auxiliary sources to a defect-detection inverse problem of optical diffraction microscopy

Mirza Karamehmedović
mirza@iwt.uni-bremen.de
Department of Process and Chemical Engineering, University of Bremen, Badgasteiner Str. 3, 28359 Bremen, Germany

Mads-Peter Sørensen
m.p.soerensen@mat.dtu.dk
DTU Mathematics, Technical University of Denmark, Matematiktorvet 303S, DK-2800 Kgs. Lyngby, Denmark

Poul-Erik Hansen
peh@dfm.dtu.dk
Danish Fundamental Metrology, Technical University of Denmark, Matematiktorvet 307, DK-2800 Kgs. Lyngby, Denmark

Andrei V. Lavrinenko
alav@fotonik.dtu.dk
DTU Fotonik, Technical University of Denmark, Ørsteds Plads 345V, DK-2800 Kgs. Lyngby, Denmark

We propose a method of numerical solution of a type of inverse scattering problem that arises in the optical characterisation/quality control of nanostructures. The underlying global, ill-posed, nonlinear optimisation problem is first localised by best-fit matching of library and measured diffraction efficiency patterns. The inverse problem is then solved using piecewise linear interpolation between the best far-field matches. Finally, the results are refined, on average, by solving an additional local optimisation problem formulated in terms of the method of auxiliary sources. To illustrate the proposed method, we apply it in a concrete quantitative characterisation of a non-periodic, nano-scale grating defect, with numerically simulated measurements. It is shown that the presented procedure can solve the inverse problem with an accuracy usually thought to require rigorous electromagnetic theories. [DOI: 10.2971/jeos.2010.10021]

Keywords: method of auxiliary sources, inverse scattering, optical diffraction microscopy, nanogratings

1 INTRODUCTION

Optical Diffraction Microscopy (ODM) [1]–[5] is a non-destructive technique of characterisation of micro and nano structures embedded in materials. Here, specific features of the sample under investigation are reconstructed from the measured optical power in the scattered far field. The technique thus requires the solution of an inverse scattering problem.

In an industrial context, such as the automated quality control of nano-scale structures embedded in materials, the inverse problem needs to be solved rapidly. Also, the structures of interest are typically comparable to the wavelength of the illuminating light used in the ODM, and accuracy requirements may therefore make it necessary to treat the inverse scattering problem using the full classical electromagnetic model, rather than asymptotic formulations. Furthermore, the problem of actual interest may not be a 'full' inverse scattering problem, since it may suffice to only measure a perturbation from an otherwise well-known scatterer structure. This is the case, e.g., in the detection and measurement of small manufacturing errors in the sample under investigation. The perturbations of interest must in general be assumed to appear non-periodically in the investigated sample.

The Method of Auxiliary Sources (MAS) [6]–[15] is a numerical technique applicable in the solution of forward and inverse scattering problems, and it is a natural candidate for integration into ODM for several reasons. If applied properly, the method can be numerically extremely efficient, and it has the potential to outperform the traditional Integral Equation (IE) schemes, especially for electrically large scatterers with complicated boundary. In addition, the MAS is in general significantly easier to implement than the traditional IE schemes. Also, the MAS is based on the full electromagnetic model, and it is well-suited for solution of both periodic and non-periodic scattering problems. Finally, it can be advantageous that the optimisation problems resulting from the formulation of inverse scattering problems in terms of the MAS do not directly involve the geometry of the scatterer as an optimisation parameter. We elaborate on the above in Section 2.

The purpose of this paper is to draw attention to the MAS as a means of formulating and numerically solving those inverse scattering problems that occur in the ODM where

- the 'nominal,' or 'defect–free,' scatterer geometry and material composition are given,
- the range of the expected deviations from the nominal scatterer is well-known and relatively small, and
- the deviations are not necessarily periodic.

As a concrete example, we use a simple MAS implementation to determine a non-periodic, nano-scale grating defect based on the measured power in the scattered far field. The numerically simulated measured scattered field is compared with a library of far-field patterns. A preliminary solution of the inverse problem is obtained by piecewise linear interpolation between the three best-fit matches from the library.

Received 8 March, 2010; published 27 April, 2010 ISSN 1990-2573

Finally, to refine the results, a local optimisation problem is formulated in terms of the MAS and solved, with the above preliminary solution used as the starting guess. The example problem is two-dimensional, with transverse-electric (TE) polarised fields. The performance of the proposed method in the transverse magnetic (TM) case, as well as the three-dimensional case, is to be investigated in a future publication.

The MAS is described in some detail in Section 2. The main characteristics of the method, as well as its applicability to inverse scattering problems, are briefly compared to those of the traditional IE schemes. In Section 3, a concrete inverse scattering problem occurring in the ODM is described. Our method of solution of the inverse problem using the MAS is described in Section 4. The numerical results are presented and discussed in Section 5. Finally, Section 6 contains conclusions and suggestions for future work.

2 THE METHOD OF AUXILIARY SOURCES

Formally, the MAS is a special case of the Integral Equation/Method of Moments (IE/MoM) variational formulation of boundary problems, characterised by the choice of Dirac delta functions $\delta(\mathbf{x}-\mathbf{x}')$ for the expansion and test vectors. Formulations of the method of varying sophistication have been studied, both analytically and numerically, at least since the late 1960s, the interest being fueled to a large extent by the potential for the construction of extremely efficient algorithms for the numerical solution of direct and inverse scattering problems. It seems that the method originated with Kupradze [6]. There is a substantial and growing body of literature on the various theoretical and applied aspects of the MAS. References [7]–[10] describe the method and put it in a more general theoretical context, and [11] gives an excellent overview of various issues related to the use of the MAS in applied electromagnetics. Concrete applications of the MAS can be found in [11]–[15].

The description of the MAS in this section is restricted to applications in two-dimensional, time-harmonic electromagnetic scattering. The example given first is in direct scattering, and it is for introductory purposes only. The second example is in inverse scattering, and it is relevant to our method described in Section 4.

Figure 1 shows a generic time-harmonic electromagnetic scattering problem in the plane.

The considered fields are assumed TE-polarised (the electric field is perpendicular to the plane of the paper), so the scattering problem is scalar with respect to the electric field. A source illuminates a perfectly electrically conducting scatterer with an incident electric field E^i, and the scatterer radiates the scattered electric field E^s. The total electric field $E^{tot} = E^i + E^s$ vanishes on the surface of the scatterer. The constant k is the wavenumber $2\pi/\lambda$, where λ is the operating wavelength. If the considered problem is a *forward* scattering problem, that is, if the boundary of the scatterer is well-known and it is of interest to find the scattered field E^s, then a corresponding MAS formulation is shown in Figure 2.

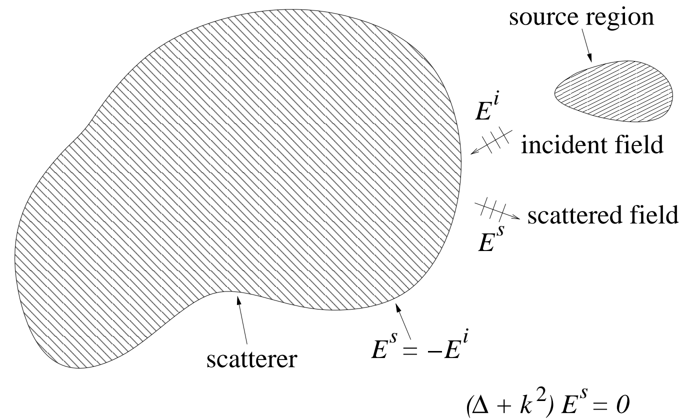

FIG. 1 A two-dimensional scattering problem, TE polarisation.

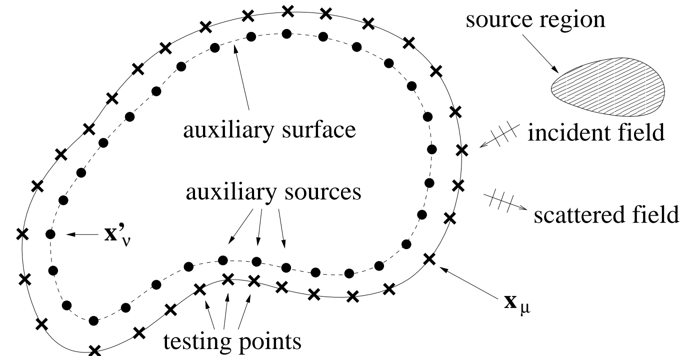

FIG. 2 A MAS setup used to solve the direct problem of Figure 1. The auxiliary sources are radiating in free space.

The scatterer is replaced by a number of so-called *auxiliary sources*, located in the interior region of the scatterer at some selected points $\mathbf{x}'_1, \ldots, \mathbf{x}'_N$, and radiating in free space. The sources are electrical line currents perpendicular to the plane of the paper, and they are to radiate an approximation to the exact scattered field (in the exterior of the scatterer). Hence the scattered field E^s is approximated in the exterior of the scatterer by a finite linear combination of the form

$$E^{MAS}(\mathbf{x}) = \sum_{\nu=1}^{N} C_\nu H_0^{(2)}(k|\mathbf{x} - \mathbf{x}'_\nu|). \tag{1}$$

Here $H_0^{(2)}$ is the Hankel function of zero order and of the second kind. The summand number ν in Eq. (1) is proportional to the radial outgoing fundamental solution of the Helmholtz operator in the plane, with singularity at $\mathbf{x}'_\nu$. Recall that, for every $\mathbf{x}' \in R^2$, the Helmholtz system

$$(\Delta+k^2)u(\mathbf{x}) = \delta(\mathbf{x}-\mathbf{x}'), \quad \mathbf{x} \in R^2, \tag{2}$$

$$\lim_{|\mathbf{x}|\to\infty} \left(|\mathbf{x}|^{1/2}(\partial_{|\mathbf{x}|}+ik)u(\mathbf{x}) \right) = 0 \tag{3}$$

has the unique solution $u(\mathbf{x}) = (i/4)H_0^{(2)}(k|\mathbf{x} - \mathbf{x}'|)$. The 'outgoing radiation condition' is given by Eq. (3). The weights (complex numbers C_ν) occurring in the linear combination Eq. (1) are determined by 'point matching', that is, by enforcing the boundary condition at selected points $\mathbf{x}_1, \ldots, \mathbf{x}_N$, on the scatterer boundary. The resulting system of linear equations, to be solved for the unknown weights, is given by

$$\sum_{\nu=1}^{N} C_\nu H_0^{(2)}(k|\mathbf{x}_\mu - \mathbf{x}'_\nu|) = -E^i(\mathbf{x}_\mu), \quad \mu = 1, \ldots, N. \tag{4}$$

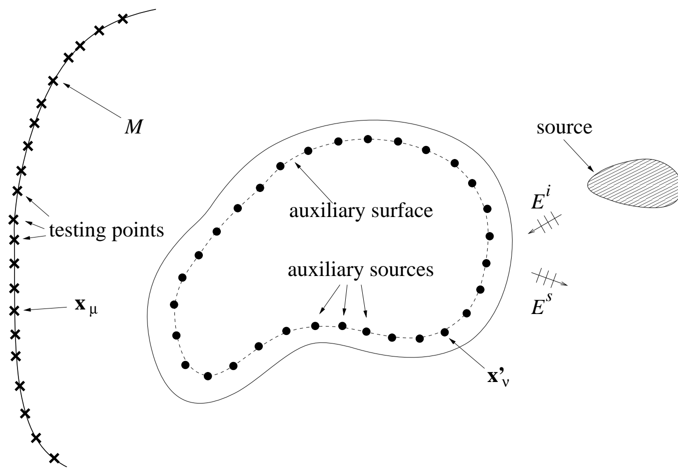

FIG. 3 A MAS setup used to solve the inverse problem of Figure 1. The auxiliary sources are radiating in free space.

Another approach [8] is to have both the complex amplitudes C_ν and the locations $\mathbf{x}'_1, \ldots, \mathbf{x}'_N$ of the auxiliary sources as unknowns, and to find these using nonlinear least-squares optimisation. The objective functional here is

$$d = \sum_{\mu=1}^{N} \left| E^i(\mathbf{x}_\mu) + \sum_{\nu=1}^{N} C_\nu H_0^{(2)}(k|\mathbf{x}_\mu - \mathbf{x}'_\nu|) \right|^2, \tag{5}$$

and the constraints are formulated to ensure that the auxiliary sources remain within the scatterer region. The number N of auxiliary sources can, in principle, also be a variable of optimisation. After solving the optimisation problem, the scattered field E^s is calculated from Eq. (1).

When solving direct scattering problems, a major issue in the practical implementation of the MAS as in Eq. (4) is the choice of the number and locations of the auxiliary sources for the given scatterer geometry and incident field. The accuracy and convergence of the method are known to be generally sensitive to this choice [11]. Without going into details, since the topic is outside the scope of this paper, we here only state that the convergence of the method is guaranteed if the auxiliary sources enclose the singularities of the analytic continuation of the scattered field inside the scatterer. When an estimate of the domain of this continuation is not available, numerical experimentation is usually needed to find a suitable spatial distribution of the auxiliary sources. For more on this topic, see Chapter 6 of [16].

If the problem in Figure 1 is an *inverse* scattering problem, then a corresponding MAS formulation is shown in Figure 3. The scattered field E^s, or, alternatively, its amplitude $|E^s|$, is here assumed well-known at the points $\mathbf{x}_1, \ldots, \mathbf{x}_N$, which may well be in the far field. *If one can*, for the particular inverse problem at hand, *relate the positions and the amplitudes of the auxiliary sources to the geometry of the scatterer*, then the reconstruction of the scatterer boundary can be attempted by minimising the difference

$$d = \sum_{\mu=1}^{N} \left| E^s(\mathbf{x}_\mu) - \sum_{\nu=1}^{N} C_\nu H_0^{(2)}(k|\mathbf{x}_\mu - \mathbf{x}'_\nu|) \right|^2, \tag{6}$$

and then interpreting the obtained best values of $C_1, \ldots, C_N$ and $\mathbf{x}'_1, \ldots, \mathbf{x}'_N$ in terms of a surface geometry. If only the power of the scattered field is measured, the difference

$$d = \sum_{\mu=1}^{N} \left| |E^s(\mathbf{x}_\mu)| - \left| \sum_{\nu=1}^{N} C_\nu H_0^{(2)}(k|\mathbf{x}_\mu - \mathbf{x}'_\nu|) \right| \right|^2. \tag{7}$$

can be sought minimised. In general, the optimisation parameters in Eqs. (6) and (7) are the positions $\mathbf{x}'_1, \ldots, \mathbf{x}'_N$ of the auxiliary sources, as well as their complex amplitudes $C_1, \ldots, C_N$. Unfortunately, the resulting nonlinear optimisation problem is typically global and very ill-posed. In analogy with the direct scattering case, it is generally difficult to choose the number, location and amplitudes of the auxiliary sources that would make a good starting guess for the optimisation. Also, it can be difficult to directly relate the best found amplitudes and positions of the auxiliary sources to an actual scatterer geometry. However, in the special case where the scatterer is known to be a relatively small perturbation of a well-known, 'nominal' scatterer, it is possible to significantly reduce the range of permissible values of the parameters of optimisation, as well as to readily interpret the results of optimisation. An example of this is given in Section 4. Even better 'reduction and interpretation' can perhaps be achieved by investigating (analytically or numerically) the analytic continuation of the scattered field to the interior of the 'nominal' scatterer and of its perturbations; this will be addressed in a future publication.

In the rest of this section, the MAS is briefly compared to the traditional IE formulations in the context of solution of inverse scattering problems.

In an IE formulation, the inverse scattering problem of Figure 1 can consist in finding a scatterer surface Γ and a surface current density J on Γ such that the far field radiated by J has the same power pattern as the measured field, and such that the total tangential electric field vanishes on Γ. (One can also place the current J on some fixed, predetermined surface Γ', as in the Kirsch-Kress method [17] and the related methods, and then look for Γ and J as described above.) Evaluation of the objective function of this nonlinear optimisation problem necessarily involves the evaluation of the intermediate scattered far fields. In this context, the MAS representation of scattered fields holds two advantages over the traditional surface integrals that originate from boundary layer potential formulations of scattering problems. First, with the MAS formulation, there is no need for numerical integration of surface currents, whereas the electric field radiated by a $\mathbf{z}$-directed, time-harmonic electric current distribution J on a surface Γ in R^2 is proportional to the integral

$$\int_\Gamma H_0^{(2)}(k|\mathbf{x} - \mathbf{x}'|) J(\mathbf{x}') d\Gamma(\mathbf{x}'), \tag{8}$$

for $\mathbf{x}$ in the exterior of Γ. The second advantage of the MAS is that the scatterer topology is identified only with the auxiliary sources, rather than with the sources *and* with a supporting surface Γ. In the abovementioned integral, the domain of integration Γ is, in general, a parameter of optimisation, and hence needs to be changed with each iteration. In conclusion, when MAS is used, the optimisation problem involves an objective function which is simply a finite sum independent of the actual geometry of the scatterer surface, as opposed to an integral taken over a generally variable surface.

The use of the MAS is not restricted to scattering problems with simple boundary conditions. The method was also found suitable for, e.g., dielectric scatterers [13] and scatterers best modeled by the Leontovich impedance boundary condition [12, 14].

3 A MODEL INVERSE PROBLEM OF OPTICAL DIFFRACTION MICROSCOPY

To illustrate our use of the MAS in the context of ODM, we here consider a concrete two-dimensional inverse scattering problem that is relevant in the practical characterisation of micro- and nano-scale surface gratings in materials.

The scatterer, a piece of corrugated silicon (rectangular grating) with complex refractive index $n_{Si} = 3.874 + i0.015$, is immersed in air and illuminated by a time-harmonic, uniform plane wave of transverse electric (TE) polarisation and unit amplitude. The incident field propagates in the negative $\mathbf{x}$ direction, and is normally incident on the grating. The operating wavelength λ is 633 nm, corresponding to illumination by a HeNe laser. The dimensions of the grating on the surface of the scatterer are $1\,\lambda \times 0.5\,\lambda$. It is desired to determine the length of one specific defective protrusion on the scatterer based on the measurement of the power in the scattered far field. The far field data are assumed available in the angle range of $\pm 30^\circ$ from normal incidence, as shown in Figure 4. The auxiliary sources and the testing points shown in Figure 4 are not part of the physical setup discussed here; these are described in Section 4.

4 SOLUTION OF THE INVERSE PROBLEM

The proposed method consists of four steps. The main idea is to identify the topology of the scatterer with the set of auxiliary sources that radiate the best approximation of the measured scattered far field power pattern. The first two steps build a library of solutions of reference direct scattering problems, and are only performed once. The last two steps need to be performed for the solution of each particular inverse scattering problem, i.e., after each particular ODM measurement.

The first step is to solve a number (say M) of direct scattering problems numerically. Each of the scattering problems models an ODM measurement and features a well-defined perturbation of the defect-free topology of the scatterer. For the nano grating of Section 3, a total of 17 direct scattering problems are solved, the length of the defective protrusion taking successive values from 0 to 2λ, with steps of 0.125λ. The resulting scattered fields, both near ($E_j^{s,near}$) and far ($E_j^{s,far}$), $j = 1, ..., M$, are stored in a library. Figure 5 shows the amplitude of one such scattered near field. We use the commercially available FEM software package COMSOL Multiphysics [18, 19] to solve the direct scattering problems.

In the second step, each stored near field is approximated by a field

$$E_j^{MAS,near}(\mathbf{x}) = \sum_{\nu=1}^{N} C_\nu^{(j)} H_0^{(2)}(k\,|\mathbf{x} - \mathbf{x}'_\nu|) \qquad (9)$$

radiated by a set of N auxiliary sources in free space. The sources are represented by their locations $\mathbf{x}'_1, \ldots, \mathbf{x}'_N$ and by their complex amplitudes $C_1^{(j)}, \ldots, C_N^{(j)}$, $j = 1, \ldots, M$. To simplify this part of the procedure, the number of sources and their locations are here fixed: for the nano grating example, we choose $N = 200$ and place the auxiliary sources at the points $\mathbf{x}'_1, \ldots, \mathbf{x}'_N$ uniformly distributed on a circle of radius 9λ, as sketched in Figure 4. The complex amplitudes $C_1^{(j)}, \ldots, C_N^{(j)}$ are calculated by point matching in the near field; in the nano grating example, the testing points are distributed uniformly on a circle of radius 9.5λ, as sketched in Figure 4. As mentioned in Section 2, the field radiated by source number μ is

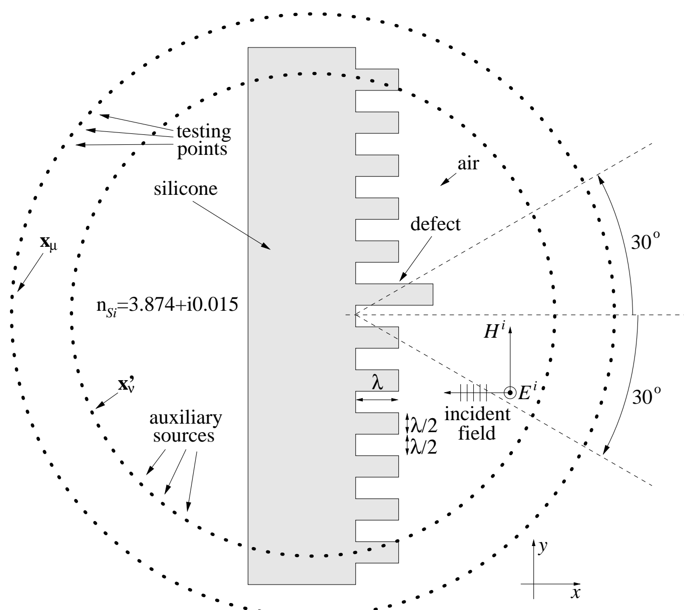

FIG. 4 The type of grating defect to be characterised.

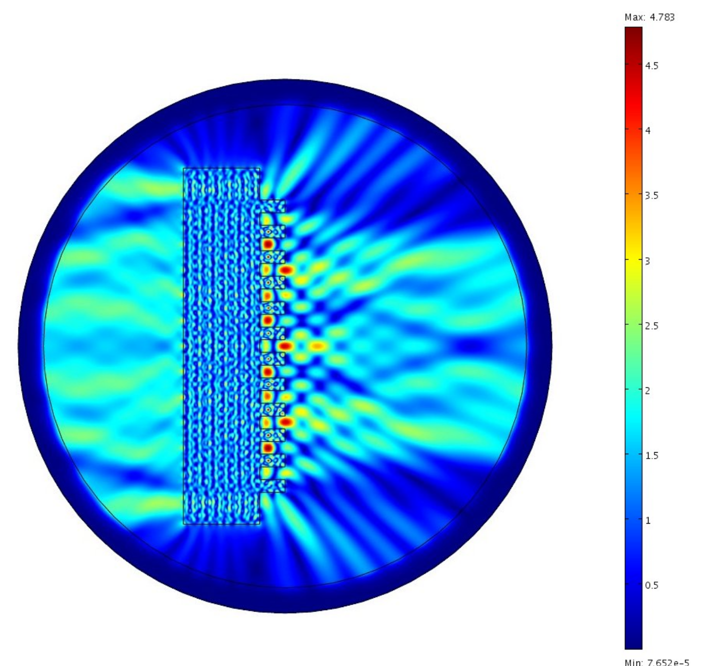

FIG. 5 The amplitude of the scattered near field for the defect-free scatterer, computed in COMSOL Multiphysics.

proportional to the radial outgoing fundamental solution of the Helmholtz operator in the plane, with singularity at $\mathbf{x}'_\mu$, that is, to the Hankel function $H_0^{(2)}(k|\cdot-\mathbf{x}'_\mu|)$ of zero order and of the second kind. For each $j=1,\ldots,M$, the (normalised) complex amplitudes are found by solving the linear system

$$\sum_{\nu=1}^{N} C_\nu^{(j)} H_0^{(2)}(k|\mathbf{x}_\mu-\mathbf{x}'_\nu|) = E_j^{s,near}(\mathbf{x}_\mu), \quad \mu=1,\ldots,N. \quad (10)$$

The distribution of the auxiliary sources and testing points shown in Figure 4 yields relatively good numerical stability. The resulting condition number for the system Eq. (10) is of the order 10^5, and the moduli of the obtained complex amplitudes $C_1^{(j)},\ldots,C_N^{(j)}$ are of the order 10^1. The normalised near-field error

$$\sqrt{\frac{\sum\left|E_j^{s,near}-E_j^{MAS,near}\right|^2}{\sum\left|E_j^{s,near}\right|^2}} \quad (11)$$

is of the order 10^{-4}, and the normalised far-field error

$$\sqrt{\frac{\sum\left||E_j^{s,far}|-|E_j^{MAS,far}|\right|^2}{\sum\left|E_j^{s,far}\right|^2}} \quad (12)$$

is found to be of the order 10^{-3} in the angle range $\pm30°$ from normal incidence. The MAS far field $E_j^{MAS,far}$ is here given by

$$E_j^{MAS,far}(\phi) = \frac{1+i}{\sqrt{\pi k}}\sum_{\nu=1}^{N} C_\nu^{(j)} \exp\left(ik|\mathbf{x}'_\nu|\cos(\phi-\phi'_\nu)\right), \quad (13)$$

where ϕ is the observation angle and ϕ'_ν the angular coordinate of the auxiliary source no. ν. Better approximation of the fields can be achieved by using more than 200 auxiliary sources and matching points.

The complex amplitudes of the sources are added to the library as vectors $\mathbf{C}^{(j)}=(C_1^{(j)},\ldots,C_N^{(j)})$ representing the respective scatterer defects. In the third step of the proposed method, the actually measured far-field amplitude $|E^{m,far}|$ is matched with the library entries $|E_j^{s,far}|$. A library entry $|E_k^{s,far}|$ is identified that minimises a distance functional of the form $\sum\left||E^{m,far}|-|E_j^{s,far}|\right|^2$. For the nano grating example, all measured fields are simulated numerically, and the matching of measured and library fields is done over the angle interval of $\pm30°$ from normal incidence. A total of 960 uniformly distributed far-field matching points are used; it is probably possible to use significantly fewer matching points with only a very small decrease in the accuracy of the method. Since the field $E_k^{s,far}$ is associated with a well-defined perturbation of the scatterer, the far-field matching gives the first, 'coarse' solution of the inverse problem. This solution is refined by piecewise linear interpolation: the functionals

$$\sum\left||E^{m,far}|-|(1+t)E_k^{s,far}-tE_{k-1}^{s,far}|\right|^2 \quad (14a)$$

and $$\sum\left||E^{m,far}|-|(1-t)E_k^{s,far}+tE_{k+1}^{s,far}|\right|^2 \quad (14b)$$

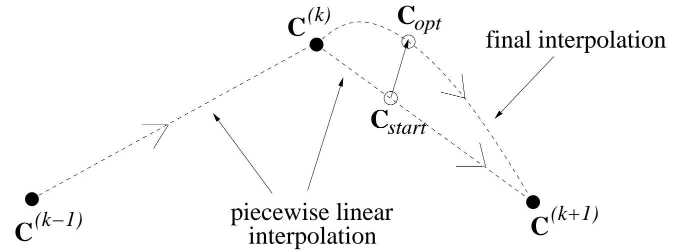

FIG. 6 Interpolating the sets of auxiliary sources.

are minimised with respect to $t\in[-1,0]$ and $t\in[0,1]$, respectively. It is here assumed that the library entries are sufficiently close such that the overall best value of t can be interpreted as a linear measure of the perturbation of the scatterer. For the nano grating example, a best far field match corresponding to the perturbation of -0.25λ and the best value of t found to be 0.296 results in the estimate $-0.25\lambda+0.125\lambda\cdot0.296=-0.213\lambda$ for the perturbation.

In the final, fourth step of the proposed method, the auxiliary source amplitude vector $\mathbf{C}_{start}=(1+t)\mathbf{C}^{(k)}-t\mathbf{C}^{(k-1)}$ (or $\mathbf{C}_{start}=(1-t)\mathbf{C}^{(k)}+t\mathbf{C}^{(k-1)}$, depending on the sign of the best t) is calculated using the above best values of t and k. Also, Gram-Schmidt orthonormalisation is performed on the set $\{\mathbf{C}^{(1)},\ldots,\mathbf{C}^{(M)}\}$ to obtain an orthonormal basis $\{\mathbf{v}_j\}$ of the d-dimensional real subspace of C^N spanned by the library source amplitude vectors (it holds that $d\leq\min\{M,2N\}$). Finally, the vector $\mathbf{C}_{start}$ is used as the starting guess in the minimisation of the functional $\sum\left||E^{m,far}|-|E_{s_1,\ldots,s_d}^{MAS,far}|\right|^2$ with respect to the reals $s_1,\ldots,s_d$. Here, $E_{s_1,\ldots,s_d}^{MAS,far}$ is the far field radiated by the set of auxiliary sources described by the amplitude vector $\mathbf{C}(s_1,\ldots,s_d)=\mathbf{C}_{start}+\sum s_\mu\mathbf{v}_\mu$ and located at $\mathbf{x}'_1,\ldots,\mathbf{x}'_N$:

$$E_{s_1,\ldots,s_d}^{MAS,far}(\phi)=\frac{1+i}{\sqrt{\pi k}}\sum_{\nu=1}^{N} C_\nu(s_1,\ldots,s_d)\exp\left(ik|\mathbf{x}'_\nu|\cos(\phi-\phi'_\nu)\right). \quad (15)$$

For the nano grating example, we employ the freely available Ipopt optimisation software [20] to find the 17 coefficients s_μ (in contrast, 400 optimisation parameters would be needed for direct optimisation with respect to the real and the imaginary parts of the complex amplitudes of the 200 auxiliary sources used in the nano grating example). We use unconstrained optimisation with a maximum of only 5 iterations, and the process takes about 30 sec of CPU time (the objective and gradient functions are implemented in MATLAB). This optimisation shows numerical convergence, so better overall results might be achieved with more iterations. After an optimum amplitude vector $\mathbf{C}_{opt}$ is found, a second-degree polynomial of one real variable and with values in C^N is constructed such that it successively intersects the points $\mathbf{C}^{(k-1)}$, $\mathbf{C}_{opt}$ and $\mathbf{C}^{(k)}$ if the above best t is nonpositive, or the points $\mathbf{C}^{(k)}$, $\mathbf{C}_{opt}$ and $\mathbf{C}^{(k+1)}$ if $t>0$ (see Figure 6 for an illustration). The perturbation in the scatterer is now estimated using relative lengths of the relevant curve segments traced in C^N by the polynomial interpolant. For the above nano grating with $t=0.296$, the lengths of the curve segments between $\mathbf{C}^{(7)}$ and $\mathbf{C}_{opt}$, as well as between $\mathbf{C}^{(7)}$ and $\mathbf{C}^{(8)}$, are 20.21 and 65.68, respectively, and the perturbation is estimated to be $-0.25\lambda+0.125\lambda\cdot20.21/65.68=-0.2115\lambda$.

actual perturbation	far-field estimate	estimate after interpolation	estimate after optimisation
-0.2000	-0.2500	-0.2181	-0.2163
-0.1875	-0.2500	-0.2130	-0.2115
-0.0500	0.0000	-0.0012	-0.0254
0.1000	0.1250	0.1260	0.1528
0.2000	0.2500	0.2948	0.2954
0.3125	0.3750	0.3750	0.3491
0.4000	0.3750	0.3750	0.3499
0.6100	0.6250	0.6249	0.5998
0.6875	0.6250	0.6345	0.6546
0.8125	0.8750	0.8750	0.8360
0.9000	0.8750	0.8925	0.9030

TABLE 1 Actual perturbations and estimates.

It is seen from Eq. (13) that the initial, piecewise linear interpolation of the far fields can be understood as an approximate piecewise linear interpolation between the auxiliary source vectors $\mathbf{C}^{(k-1)}$, $\mathbf{C}^{(k)}$ and $\mathbf{C}^{(k+1)}$, since, e.g.,

$$(1+t)E_k^{s,far}(\phi)-tE_{k-1}^{s,far}(\phi) \approx \frac{1+i}{\sqrt{\pi k}}\sum_{\nu=1}^{N}\left((1+t)C_\nu^{(k)}-tC_\nu^{(k-1)}\right)\exp\left(ik|\mathbf{x}'_\nu|\cos(\phi-\phi'_\nu)\right). \quad (16)$$

This is why we indicate the linear interpolation in Figure 6. Also, while the library matching and the subsequent piecewise linear interpolation are done directly on the far field data, without any use of a MAS formulation, the final optimisation generally changes the individual parameters $C_\nu^{(j)}$ independently of each other; thus the last step indeed makes use of the MAS expansion of the scattered field.

5 NUMERICAL RESULTS

Tables 1, 2 and 3 summarise the numerical results obtained for the nano grating example. The 'after interpolation' column refers to the initial, piecewise linear interpolation. The column labeled 'after optimisation' refers to the final step of the proposed method, where a MAS-formulated optimisation problem is solved and where second-order interpolation is used. All values in Table 1 are given in wavelengths λ and are rounded to 4 decimal places. A perturbation of -0.2λ corresponds to the case where the defective protrusion is 0.8λ long, and similarly for the other values. In Table 2, the error in the j'th estimate $\tilde{l}_j$ of the actual perturbation l_j is calculated as $\varepsilon_j = 100(\tilde{l}_j - l_j)$, if both l_j and $\tilde{l}_j$ are given in wavelengths λ. The 'standard deviation' is calculated as $\sigma = (\sum \varepsilon_j^2/11)^{1/2}$. Both values are rounded to 2 decimal places. In Table 3 the far-field error after library matching is found as

$$100 \cdot \sqrt{\sum \left| |E^{m,far}| - |E_k^{s,far}| \right|^2 / \sum |E^{m,far}|^2}, \quad (17)$$

and similarly for the other two error columns. With the present resolution of the library, the far field matching results in reasonable initial guesses in all 11 cases. The error in the resulting estimates does not exceed 10% of the wavelength λ, and this is also the case for the interpolation and optimisation data sets. The subsequent piecewise linear interpolation reduces both the average absolute value and the standard deviation of the error in the estimates. Also, in all 11 considered cases, the far-field error after the initial interpolation is either less than or equal to the far-field error obtained after library matching. Use of the MAS-formulated optimisation, and the subsequent second-degree polynomial interpolation, further reduces the far-field error, the average absolute value of the estimate error, and the standard deviation of the estimate error. Compared to the interpolation estimates, the magnitude of the error is reduced in 8 of the shown 11 cases. Of course, the scatterer perturbations directly represented in the library are measured with zero error, which in principle improves the overall accuracy estimate for the method. However, we must

actual perturbation	error / λ (%) after library matching	error / λ (%) after interpolation	error / λ (%) after optimisation
-0.2000	-5.00	-1.81	-1.63
-0.1875	-6.25	-2.55	-2.40
-0.0500	5.00	4.88	2.46
0.1000	2.50	2.60	5.28
0.2000	5.00	9.48	9.54
0.3125	6.25	6.25	3.66
0.4000	-2.50	-2.50	-5.01
0.6100	1.50	1.49	-1.02
0.6875	-6.25	-5.30	-3.29
0.8125	6.25	6.25	2.35
0.9000	-2.50	-0.75	0.30
average absolute value	4.45	3.99	3.36
standard deviation	4.79	4.72	4.15

TABLE 2 Errors in the estimates.

actual perturbation	far-field error (%) after library matching	far-field error (%) after interpolation	far-field error (%) after optimisation
-0.2000	24.76	15.88	9.88
-0.1875	25.66	16.11	10.27
-0.0500	7.51	7.51	2.84
0.1000	7.01	6.90	4.68
0.2000	11.81	9.69	1.73
0.3125	5.97	5.97	3.00
0.4000	2.42	2.42	0.89
0.6100	1.36	1.36	0.48
0.6875	8.48	8.47	3.80
0.8125	20.69	20.69	5.37
0.9000	4.23	3.97	1.57
average absolute value	10.90	9.00	4.05

TABLE 3 Error in the reconstructed far-field amplitude relative to the measured far field.

also point out the fluctuation in the magnitude of the estimate error from case to case.

6 CONCLUSIONS AND FURTHER WORK

It was here demonstrated that the MAS can be used in an ODM setting for efficient measurement of non-periodic defects on nano scale. The method was tested on a concrete relevant inverse problem, where the elongation of a specific protrusion in a nano-scale grating was estimated. A MAS-based optimisation resulted in a lower average absolute value and a lower standard deviation of the estimate error, compared to simple piecewise linear interpolation of the far fields.

The presented numerical implementation involves implicit choices for many different parameters, and its performance can therefore likely be further improved. We do not claim here that the implementation is optimal; its purpose is solely to demonstrate the feasibility of the proposed approach to the inverse problems that occur in ODM.

Regarding further work, we mention that all three sets of estimates (matching, interpolation and optimisation) show statistically significant errors for several perturbations in the range from $-\lambda$ to -0.3λ; further investigation is thus needed for geometries where the perturbation is 'buried' in the scatterer structure. It is also of interest to test the proposed method on the nano grating inverse problem in the transverse magnetic (TM) case. Furthermore, the effect of measurement noise on the accuracy of the method needs to be investigated. In general, the choice of the location of the auxiliary sources can significantly influence the well-posedness of the final optimisation problem, and it is of interest to find favourable auxiliary source distributions, dependent on the considered scatterer, that make the method numerically stable and that even improve its accuracy. Next, it might be useful to investigate the effect of resonances induced in the measured structures on the performance of the method. Finally, it is relevant to generalise the presented method to three-dimensional, polychromatic, time-domain measurements.

ACKNOWLEDGEMENTS

We acknowledge the financial support from the innovation consortium FINST under the Danish Agency for Science, Technology and Innovation, as well as from the Dept. of Process and Chemical Engineering, University of Bremen, Germany.

References

[1] N. Agersnap, P.-E. Hansen, J. C. Petersen, J. Garnaes, N. Destouches, and O. Parriaux, "Critical dimension metrology using optical diffraction microscopy" Proc. SPIE **5965**, 68–78 (2005).

[2] F. Borsetto, K. Carneiro, I. Davi, J. Garnaes, J. C. Petersen, N. Agersnap, P.-E. Hansen, J. Holm, and L. H. Christensen, "Profile characterization with combined atomic force (AFM) and optical diffraction microscopy (ODM)" in *Proceedings of the euspen 7th International Conference and 8th General Meeting of the European Society for Precision Engineering and Nanotechnology* (Baaden, 2006).

[3] J. Garnaes, P.-E. Hansen, N. Agersnap, I. Davi, J. C. Petersen, A. Kühle, J. Holm, and L. H. Christensen, "Determination of submicrometer high aspect ratio grating profiles" Proc. SPIE **5878**, 1–9 (2005).

[4] J. Garnaes, P.-E. Hansen, N. Agersnap, J. Holm, F. Borsetto, and A. Kühle, "Profiles of high aspect ratio grating determined by optical diffraction microscopy and atomic force microscopy" Appl. Opt. **45**, 3201–3212 (2006).

[5] P.-E. Hansen, and L. Nielsen, "Combined optimization and hybrid scalar-vector diffraction method for grating topography parameters determination" Mater. Sci. Eng. B **165**, 165–168 (2009).

[6] V. D. Kupradze, "On the approximate solution of problems of mathematical physics" Russ. Math. Surv.+ **22**, 59–107 (1967).

[7] G. Fairweather, and A. Karageorghis, "The method of fundamental solutions for elliptic boundary value problems" Adv. Comput. Math. **9**, 69–95 (1998).

[8] G. Fairweather, A. Karageorghis, and P. A. Martin, "The method of fundamental solutions for scattering and radiation problems" Eng. Anal. Bound. Elem. **27**, 759–769 (2003).

[9] A. Doicu, Y. A. Eremin, and T. Wriedt, *Acoustic and Electromagnetic Scattering Analysis Using Discrete Sources* (Academic Press, 2000).

[10] T. Wriedt (ed.), *Generalized Multipole Techniques for Electromagnetic and Light Scattering* (Elsevier, 1999).

[11] D. I. Kaklamani, and H. T. Anastassiu, "Aspects of the method of auxiliary sources (MAS) in computational electromagnetics" IEEE Antenn. Propag. Mag. **44**, 48–64 (2002).

[12] H. T. Anastassiu, D. I. Kaklamani, D. P. Economou, and O. Breinbjerg, "Electromagnetic scattering analysis of coated conductors with edges using the method of auxiliary sources (MAS) in conjunction with the standard impedance boundary condition (SIBC)" IEEE Trans. Antenn. Propag. **50**, 59–66 (2002).

[13] Y. Leviatan, A. Boag, and A. Boag, "Analysis of TE scattering from dielectric cylinders using a multifilament magnetic current model" IEEE Trans. Antenn. Propag. **36**, 1026–1031 (1988).

[14] M. Karamehmedovic, and O. Brienbjerg, "Application of the method of auxiliary sources for the analysis of plane-wave scattering by impedance spheres" in *Proceedings of the 2002 International Conference on Mathematical Methods in Electromagnetic Theory MMET02*, 499–501 (Kiev, 2002).

[15] M. Karamehmedovic, and O. Brienbjerg, "A convergent method of auxiliary sources for two-dimensional impedance scatterers with edges" in *Proceedings of the 16th International Conference on Applied Electromagnetics and Communications*, 46–49 (Dubrovnik, 2001).

[16] B. Sternin, and V. Shatalov, *Differential Equations on Complex Manifolds* (Kluwer Academic Publishers, 1994).

[17] D. Colton, and R. Kress, *Inverse Acoustic and Electromagnetic Scattering Theory* (Springer, 1998).

[18] COMSOL Multiphysics demonstration CD-ROM can be requested at http://www.comsol.com.

[19] W. B. J. Zimmerman, *Multiphysics Modelling with Finite Element Methods* (World Scientific, 2006).

[20] A. Wächter, and L. T. Biegler, "On the implementation of a primal-dual interior point filter line search algorithm for large-scale nonlinear programming" Math. Program. **106**, 25–57 (2006).